Dalton Transactions

PAPER

View Article Online
View Journal | View Issue

Cite this: *Dalton Trans.*, 2025, **54**, 5301

Synthesis and large crystal growth of a family of mixed-anionic methanesulfonate salts by anionic site-substitution: $Na_5(SO_3CH_3)_4(X)$ ($X = BF_4^-, ClO_4^-, PF_6^-, I^-$)†

Eric A. Gabilondo and P. Shiv Halasyamani *

Received 27th January 2025,
Accepted 5th March 2025

DOI: 10.1039/d5dt00223k

rsc.li/dalton

Four new mixed-anionic sodium methanesulfonate compounds were synthesized – $Na_5(SO_3CH_3)_4(X)$ (X = (**I**) BF_4^-, (**II**) ClO_4^-, (**III**) PF_6^-, and (**IV**) I^-). Compounds **I–III** were grown as centimeter-size crystals under ambient conditions. Metal methanesulfonates (*i.e.*, MSO_3CH_3 or $M(SO_3CH_3)_2$) are proposed as potential high-performance nonlinear optical materials owing to their large calculated bandgaps, local anisotropy, and large polarization. However, there are few experimental reports in the literature. The present study involves using anionic substitution as a structure building strategy to discover new complex metal methanesulfonates. The new compounds, $Na_5(SO_3CH_3)_4(X)$, where X = (**I**) $[BF_4]^-$, (**II**) $[ClO_4]^-$, (**III**) $[PF_6]^-$, and (**IV**) $[I]^-$ crystallize in the monoclinic space groups *P*2/*n* or *I*2/*m*, and are prepared as (**I–III**) high-quality and centimeter-sized crystals grown at ambient conditions, whereas millimeter-sized crystals of **I**, **II**, and **IV** could be prepared in high yields by hydrothermal synthesis. **I–III** have wide optical transparency from 400–1100 nm and λ_{abs} of ≤210 nm. **I–III** are each highly soluble in water, air stable for several months, and thermally stable below 350 °C. These data suggest that ionic-substitution is a viable method of discovering new and complex metal methanesulfonate salts with diverse properties.

1. Introduction

Compounds containing mixed-anionic groups are of essential importance in materials applications owing to the remarkable tuneability of both crystal structure and properties.[1–4] Some of these recent applications include using functional groups with stereoactive lone pairs[5,6] (*e.g.*, $[SeO_3]^{2-}$, $[BiO_6]^{9-}$) or polar tetrahedra[7,8] (*e.g.*, $[PO_3F]^{2-}$ and $[BO_3F]^{4-}$) to break symmetry and form acentric crystal structures for applications as nonlinear optical (NLO) materials.[9,10] Similarly, anionic substitution facilitates the improvement of materials such as the improved crystal growth and reduced toxicity in $Cs_3Zn_6B_9O_{21}$,[11] the $AZn_2BO_3X_2$ family,[12] or $Rb_3Ba_3Li_2Al_4B_6O_{20}$,[13] *versus* the famous NLO crystal $KBe_2BO_3F_2$ that requires the use of toxic BeO in the synthesis.[14] As a result, the substitution of anionic groups within structure classes is an effective method for materials discovery, and may be used to create new compounds with improved properties.

Metal methanesulfonates, *i.e.*, MSO_3CH_3 or $M(SO_3CH_3)_2$, have been recently predicted as a potential new class of NLO materials owing to their calculated larger optical bandgaps and polarizability of the $[SO_3CH_3]^-$ anion compared to commonly used functional groups such as $[IO_3]^-$, $[SO_4]^{2-}$, and $[BO_3]^{3-}$.[15] This has been empirically demonstrated in the case of $Ba(SO_3CH_3)_2$ as a NLO candidate crystal.[16] Most reported metal methanesulfonates are centrosymmetric (55 out of 65 as of Jan. 2025),[17] however, and cannot be used as NLO materials. As previously mentioned, adding additional anionic groups could lower the symmetry and allow NLO properties to flourish. There are currently only three mixed-metal methanesulfonates reported, $M[Au(SO_3CH_3)_4]$ ($M = Li^+, Na^+, Rb^+$),[18] and only five mixed-anionic methanesulfonates – $(Bi(Se/Te)O_3)(SO_3CH_3)$, $Ba(SO_3CH_3)(BF_4)$, $Ba_2(SO_3CH_3)_3(BF_4)(H_2O)_3$,[19] and $Na(S(OH)_3CH_3)(BO_3)$.[20] Each of these compounds exhibit unique structures and properties in contrast to their simple binary salts and respective hydrates, *e.g.* $Ba(SO_3CH_3)_2$, $Ba(SO_3CH_3)_2\cdot 1.5H_2O$, and $NaSO_3CH_3$. The dearth of reported complex metal methanesulfonates requires further exploration.

Many binary metal methanesulfonates, *e.g.*, $LiSO_3CH_3$ and $Ba(SO_3CH_3)_2$,[15,21] crystallize as layered structures that are ripe targets for ion-substitution or -exchange as a rapid discovery method for lamellar compounds.[22,23] For example, sodium

---

University of Houston, Department of Chemistry, Houston, TX 77204-5003, USA. E-mail: psh@uh.edu

† Electronic supplementary information (ESI) available. CCDC 2417057–2417060. For ESI and crystallographic data in CIF or other electronic format see DOI: https://doi.org/10.1039/d5dt00223k

methanesulfonate ($NaSO_3CH_3$), is structurally comprised of $[Na_5(SO_3CH_3)_4]_n^+$ 2D-layers with an intercalated $[SO_3CH_3]_n^-$ anion.[24] In the present work, we investigate $NaSO_3CH_3$ as an example structure-class to perform interlayer site-substitution to discover new mixed-anionic metal methanesulfonates. $NaSO_3CH_3$ is simple and low-cost to prepare as large crystals and is generally easier to handle compared to its more hygroscopic counterparts. We discuss below the discovery of four new and isostructural mixed-anionic metal methanesulfonates, $Na_5(SO_3CH_3)_4(X)$, where X = (**I**) $[BF_4]^-$, (**II**) $[ClO_4]^-$, (**III**) $[PF_6]^-$, and (**IV**) $[I]^-$. The known $NaSO_3CH_3$ compound, or (**V**) X = $SO_3CH_3^-$ for brevity, was similarly prepared for direct comparison. The new compounds crystallize in centrosymmetric monoclinic space groups *P*2/*n* (no. 13) (**I**, **II**, **IV**) or *I*2/*m* (no. 12) (**III**) derived from the structure of (**V**) that crystallizes in the orthorhombic space group *Pbma* (no. 57). Each compound could be prepared in high purity through hydrothermal methods, whereas compounds **I**–**III** could be grown as high-quality centimeter-sized crystals under ambient conditions. This manuscript discusses their preparation, crystal structure, optical properties, and thermal stabilities.

2. Experimental

2.1. Reagents

Na_2CO_3 (98%, Alfa Aesar), NaCl (99%, EM Chemicals), HSO_3CH_3 (70 w/w% solution, Sigma-Aldrich), $NaBF_4$ (97%, Alfa Aesar), $HClO_4$ (60–62% solution, Alfa Aesar), KPF_6 (99% min, Alfa Aesar), and NH_4I (99%, Sigma-Aldrich), and acetonitrile (VWR) were used as reagents with no additional purification.

Caution: Perchloric acid (CAS#: 7601-90-3) is a strong oxidizer, potentially explosive, and should be handled with great care. All usage should be carried out in a fume hood specially rated for $HClO_4$ in case of spills.

2.2. Synthesis

Compounds **I**, **II**, and **IV** were synthesized using hydrothermal methods. Nonstoichiometric mixtures of Na_2CO_3, HSO_3CH_3 solution, and X (*i.e.*, (**I**) $NaBF_4$, (**II**) $HClO_4$, or (**IV**) NH_4I) were required for each reaction. The loadings were (**I**) 1.2 g (11.3 mmol) Na_2CO_3, 0.84 g (7.7 mmol) $NaBF_4$, and 1.5 mL (14.9 mmol) HSO_3CH_3; (**II**) 1.15 g (10.9 mmol) Na_2CO_3, 0.34 mL (3.1 mmol) $HClO_4$, and 0.5 mL (5.0 mmol) HSO_3CH_3; (**IV**) 1.00 g (9.4 mmol) Na_2CO_3, 0.547 g (3.8 mmol) NH_4I, and 1.5 mL (14.9 mmol) HSO_3CH_3. The reagent mixtures each had 1 mL of water added and were loaded into separate 23 mL Teflon-lined autoclaves. The autoclaves were heated at a rate of 1 °C min^{-1} to 220 °C for 96 h (4 days), and a cooled to room temperature at a rate of 0.1 °C min^{-1}. The products were vacuum filtered and rinsed with 5 mL of acetonitrile to remove excess solvent adhered to the surface prior to air drying. Each reaction produced mm-scale crystals that could be mechanically separated and then cut for single-crystal X-ray diffraction. Compounds **I**, **II**, and **IV** each had yields of 78%, 79%, and 70%, respectively, with respect to the X-containing reagent. Compound **III** could not be prepared under similar reaction conditions.

Large crystal growth of compounds **I**–**III** and **V** was performed through solvent evaporation at ambient conditions by mixing Na_2CO_3, and X (*i.e.*, (**I**) $NaBF_4$, (**II**) $HClO_4$, or (**III**) KPF_6) in 10 mL of HSO_3CH_3 and 30 mL of deionized water giving a total volume of approximately 45 mL in each reaction. Loadings were (**I**) 2.428 g (22.9 mmol) Na_2CO_3 and 1.6836 g (15.3 mmol) $NaBF_4$; (**II**) 2.3 g (21.7 mmol) Na_2CO_3 and 0.679 mL (6.2 mmol) $HClO_4$; (**III**) 2.04 g (34.9 mmol) NaCl, 1.28 g (7.0 mmol) KPF_6; (**V**) 2.5 g (23.6 mmol) Na_2CO_3. Plastic containers were used for compounds **I** and **III** as the $[BF_4]^-$ and $[PF_6]^-$ anions attack glass. Each liquid mixture was placed uncovered on a benchtop in air except compound **III** which was in a fume hood rated for $HClO_4$. Centimeter-scale (**I**, **II**, **V**) plate and (**III**) rectangular prism crystals appeared after 1–2 weeks. Compound **IV** could not be prepared under similar conditions. Crystals were mechanically separated from the mother liquor before vacuum filtration and rinsing with 10 mL of acetonitrile to remove the excess. All large crystals are stable in air for several months.

2.3. Structural determination

Single-crystal X-ray diffraction (SCXRD) for compounds **I**–**IV** was performed with crystals obtained from hydrothermal synthesis described above. Data was collected using a Bruker SMART X-ray diffractometer using with a CCD detector and graphite monochromator, controlled through the APEX2 software.[25] Data collection was obtained with a Mo Kα source (λ = 0.71073 Å) at 298 K. The SAINT and SADABS programs were used to integrate the collected frames and to correct for absorption, respectively, and the space group confirmed by the XPREP software.[26,27] The structure solution was obtained by using the ShelXT direct method and intrinsic phasing prior to structural refinement with ShelXL in the Olex2-1.5 software package.[28–31] The PLATON and ADDSYM software packages were used to check for missing symmetry elements.[32–34] Bond-valence summations (BVS) were calculated using method described by Brown[35] with parameters obtained from the International Union of Crystallography and reported crystal structures containing X-group motifs.[36–40] The structure refinement summary for compounds **I**–**IV**, BVS, bond lengths, and bond angles, are contained in Table 1 and Tables S1–S5 in the ESI.† The crystallographic information files (cifs) for compounds **I**–**IV** are provided as part of the electronic ESI.† The crystal structure for compound **V** has been previously reported elsewhere (CCDC no. 1105562).[24] All structural models were constructed using the VESTA software.[41]

All powder X-ray diffraction (PXRD) data was collected on ground crystals with a PANalytical Empyrean diffractometer using Cu Kα radiation (λ_1 = 1.54059 Å, λ_2 = 1.54432 Å, I_2/I_1 = 0.5) in Bragg–Brentano geometry on a fixed glass plate. Indexing of the primary crystal facet was observed by mounting a crystal flat on the sample stage position and rotating the crystal 90° before subsequent scans. PXRD data sets from the indexing method are provided in Fig. S7 in the ESI.†

Table 1 Summary of crystal data and structural refinements for compounds **I–IV**. All data were collected using a Mo Kα (λ = 0.71073 Å) source at 298 K

Formula	$Na_5(SO_3CH_3)_4(BF_4)$	$Na_5(SO_3CH_3)_4(ClO_4)$	$Na_5(SO_3CH_3)_4(PF_6)$	$Na_5(SO_3CH_3)_4(I)$
Crystal size (mm)	0.20 × 0.30 × 0.50	0.40 × 0.40 × 0.35	0.15 × 0.13 × 0.05	0.05 × 0.10 × 0.12
Formula weight (g mol^{-1})	582.14	594.78	640.30	622.23
Crystal system	Monoclinic	Monoclinic	Monoclinic	Monoclinic
Space group	$P2/n$ (13)	$P2/n$ (13)	$I2/m$ (12)	$P2/n$ (13)
a (Å)	12.524(4)	12.6653(7)	12.9030(3)	12.4118(4)
b (Å)	5.534(1)	5.5400(3)	5.5449(1)	5.5158(2)
c (Å)	15.001(4)	15.0037(9)	15.1892(6)	14.9258(5)
β (°)	102.878(4)	103.263(3)	103.946(2)	102.489(2)
V (Å^3)	1013.5(5)	1024.67(10)	1054.69(5)	997.66(6)
Z	2	2	2	2
D_{calc} (g cm^{-1})	1.907	1.928	2.016	2.071
μ (mm^{-1})	0.664	0.773	0.734	2.181
GooF on F^2	1.050	1.049	1.046	1.009
R_1/wR_2 [$I > 2\sigma(I)$]^a	0.0288/0.0776	0.0269/0.0781	0.0311/0.0710	0.0293/0.0716
R_1/wR_2 (all data)^a	0.0358/0.0819	0.0281/0.0813	0.0407/0.0760	0.0575/0.0716
F(000)	584	600	640	608
Largest diff. peak/hole (e Å^{-3})	0.56, −0.43	0.45, −0.67	0.38, −0.35	0.60, −0.50
Reflections total, unique	9448, 2352	35337, 2567	8438, 1246	31164, 2734
R_{int}, R_σ	0.0294, 0.0215	0.0286, 0.0104	0.0349, 0.0221	0.063, 0.0296

^{a} $R_1 = \sum||F_o| - |F_c||/\sum|F_o|$; w$R_2 = \{\sum w[(F_o)^2 - (F_c)^2]^2/\sum w[(F_o)^2]^2\}^{1/2}$.

Scanning electron microscopy (SEM) and energy dispersive X-ray spectroscopy (EDS) were used to confirm crystal homogeneity and elemental composition. SEM/EDS was performed using an Axia-ChemiSEM (Thermo Fisher) equipped with EDS and cathodoluminescense detectors. SEM images with EDS elemental mapping as well as the raw EDS spectra are contained in Fig. S1–S6 in the ESI.†

2.4. Thermal stability and optical characterization

The thermal stability of compounds **I–V** were determined using thermogravimetric analysis (TGA) on an EXSTAR 6300 TG/DTA. Data was collected under N_2 flow from 25–600 °C and a ramp rate of 10 °C min^{-1}. Thermal decomposition was performed by annealing each compound in an evacuated and sealed quartz tube at 600 °C for 2 h. Partial pyrolysis was investigated by annealing single-crystals of **I–IV** at 300 °C for 2 h under static vacuum. Diffuse reflectance spectroscopy was collected from 200–1200 nm on a JASCO V-770 UV-Visible/NIR spectrophotometer with a Spectralon reference. Optical bandgaps were estimated using the Tauc method and extrapolating the square of the remission function to the baseline.[42–44] Fourier-Transformed Infrared (FT-IR) spectroscopy was performed over the range of 400–4000 cm^{-1} using a Thermo Scientific Nicolet iS10 FT-IR spectrophotometer.

3. Results and discussion

3.1. Synthesis and crystal structures

The anionic groups $[BF_4]^-$, $[ClO_4]^-$, and $[PF_6]^-$, and $[I]^-$ were chosen as interlayer substituents for $NaSO_3CH_3$ as they have similar ionic radii and charge to the $[SO_3CH_3]^-$ anion although different coordination environments. Each listed anion is considered a "non-coordinating ion"[45] and possess similar charge densities (r = 2.2–2.24 Å).[46–48] We anticipate the four anionic groups have similar bonding affinities as the mesylate group. Therefore, isostructural substitution is a reasonable approach to new metal methanesulfonates. Compounds **I**, **II**, and **IV** were prepared *via* hydrothermal synthesis and large crystals of **I–III** and **V** were grown at room temperature through slow evaporation of solvent. **IV** could not be grown by solution evaporation owing to the instability of the solvated $[I]^-$ anion in the presence of oxygen. PXRD of ground crystals and photographs of **I–IV** crystals are shown in Fig. 1 and the crystal structure refinements in Table 1. As shown in Fig. 1, each crystal is single-phase and the PXRD data are in good agreement with the calculated Bragg-peaks obtained from SCXRD. The reported (**V**) $NaSO_3CH_3$ typically grows as long, rectangular platelets (Fig. S7†), while **I** and **II** have blade and angular plate habits. **III** and **IV** grow as rectangular prisms and irregular prisms, respectively. The largest single-crystals obtained for each compound were (**I**) 1.4 × 0.5 × 0.1 (**II**) 1.0 × 0.5 × 0.1, (**III**) 1 × 0.4 × 0.4, all in cm^3, and (**IV**) = 1.4 × 1.5 × 1 in mm^3. The primary facets of the cm-scale crystals for **I–III** and **V** were indexed (Fig. S7†) to the ($10\bar{1}$) (**I**, **II**), (001) (**III**), or (020) (**V**) interlayer planes, similar to their PXRD. Crystals of **IV** were too small to index, however PXRD suggests the crystal orientation is similarly layered in preference. EDS (Fig. S1–S6†) agree with the XRD-determined composition. Compounds **I**, **II**, and **IV** are highly oriented in a layered habit, increasing the intensity of the PXRD peaks corresponding to the $\{10\bar{1}\}$ planes. This is especially true in **IV**, where the ($30\bar{3}$) is significantly more intense than calculated. Crystals of **I–III** are air stable, however **IV** and all the powders are significantly hygroscopic. **IV** in general appears to leak iodine slowly into its surroundings and produces red-brown stains.

The unit cells of **I–V** as determined by SCXRD are shown in Fig. 2 with a schematic representation of the structural similarities and the local coordination environments in Fig. 3, while full crystallographic data including atomic coordinates

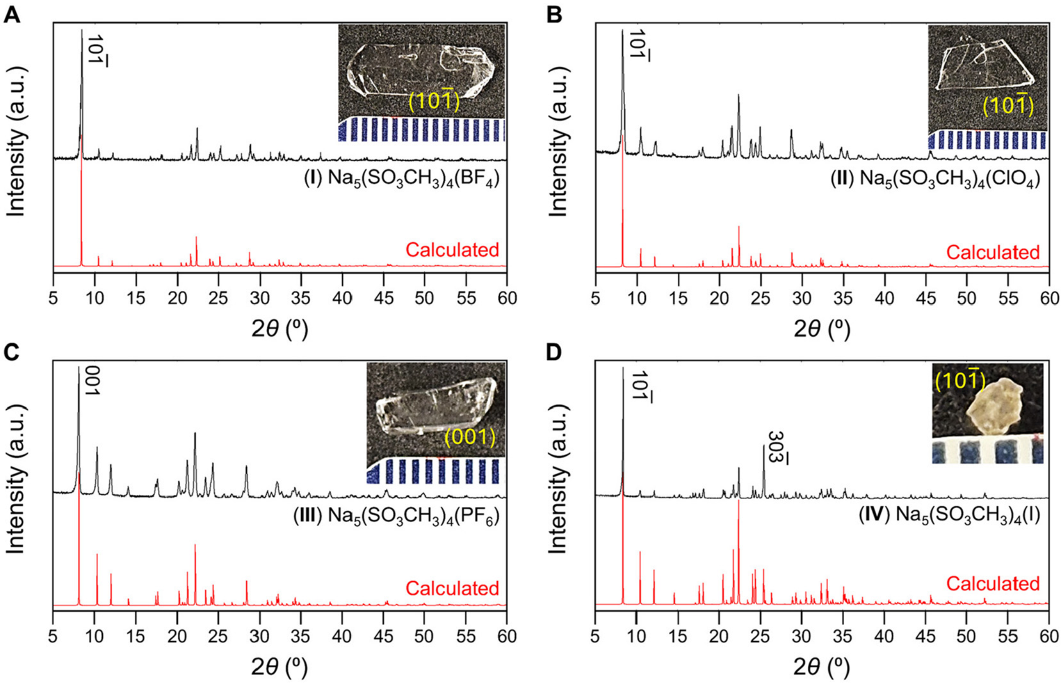

Fig. 1 PXRD of compounds (A) **I**, (B), **II**, (C) **III**, and (D) **IV** with calculated PXRD patterns (red) below. (Inset) photographs of the as-grown crystals of **I–IV** with the primary face indexed.

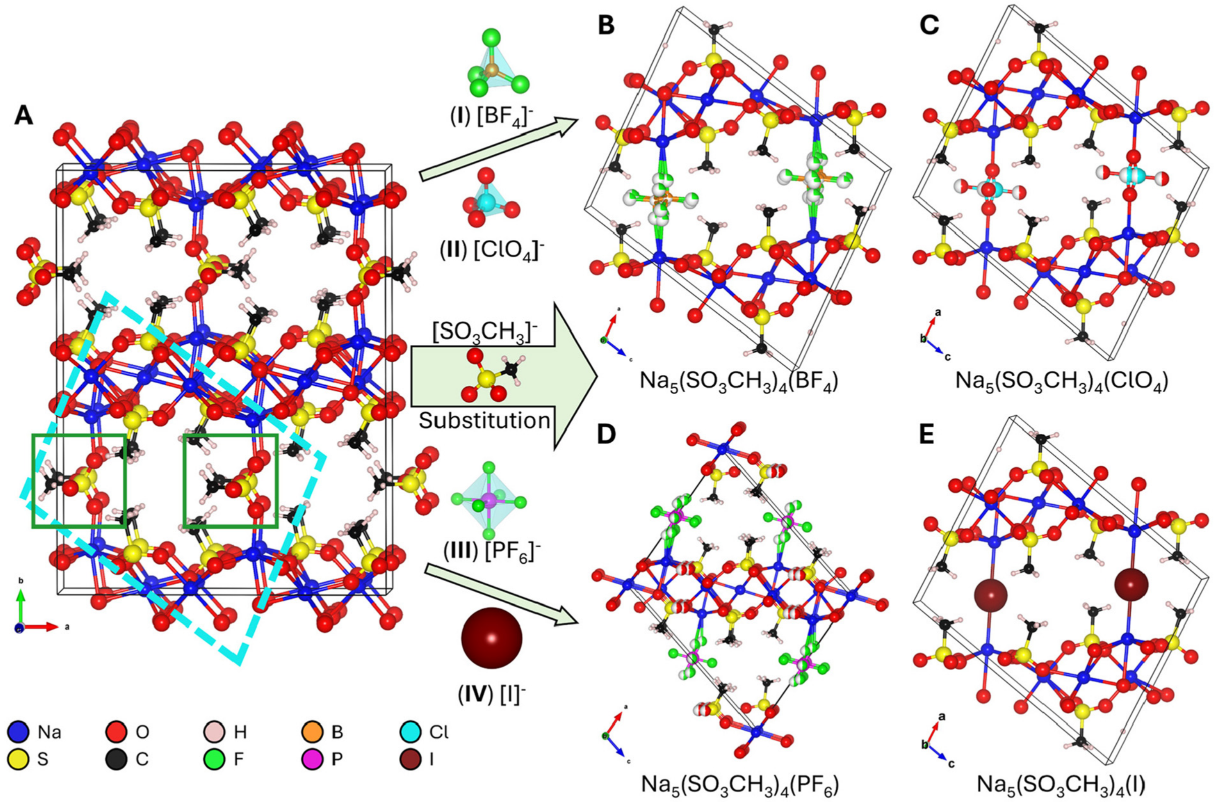

Fig. 2 Unit cells and structural evolution of $Na_5(SO_3CH_3)_4(X)$ where X = (A) (**V**) $[SO_3CH_3]^-$, (B) (**I**) $[BF_4]^-$, (C) (**II**) $[ClO_4]^-$, (D) (**III**) $[PF_6]^-$, and (E) (**IV**) $[I]^-$ through anionic substitution of the interlayer anion site. The cyan box on A shows the prototype unit cell of **I–IV** and the green boxes are the substituted crystallographic site.

bond lengths and angles are available in Table 1 and Tables S1–5.† The known **V** (Fig. 2A) crystallizes in the orthorhombic space group *Pbma* (no. 57) with lattice parameters a = 17.0713(6) Å, b = 22.0217(6) Å, and c = 5.6058(3) Å, and V = 2107.4(1) Å^3. Compounds **I**, **II**, and **IV** crystallize in the monoclinic space group *P*2/*n* (no. 13) while **III** crystallizes in *I*2/*m* (no. 12) with similar lattice parameters. Boxes drawn in Fig. 2A illustrate the structural evolution. The higher symmetry substituent-anions $[BF_4]^-$, $[ClO_4]^-$, $[PF_6]^-$, and $[I]^-$ (Fig. 2B–E) do not require multiple layers to describe since they disorder over a single site as opposed to the ordered $[SO_3CH_3]^-$. Their coordination will be discussed further below. The resulting unit cells have a reduction in volume of $\sim\frac{1}{2}$, *i.e.*, (**V**) 2107 Å^3 → (**I**) 1013 Å^3, and a reduction of overall symmetry, orthorhombic → monoclinic. The resulting lattice parameters and β-angle of **I–IV** are comparable to each other as shown in Table 1. BVS calculations (Table S1†) are in agreement with the anticipated oxidation states for each structural unit S(VI), Na(I), O^{2-}, C(IV), B(III), F^-, P(V), I^-, and Cl(VII).

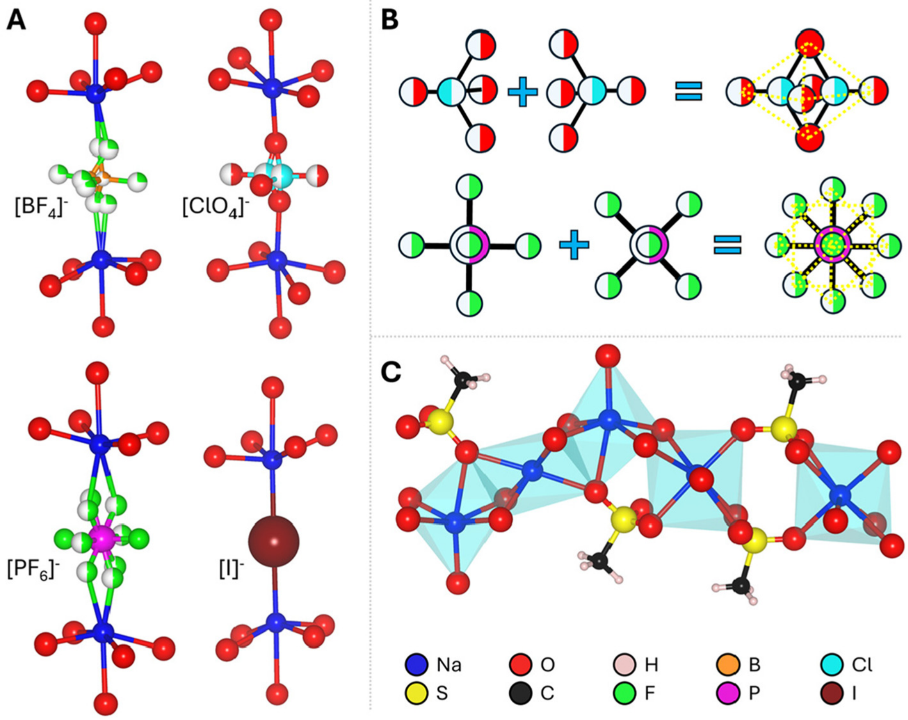

Fig. 3 (A) Interlayer anion coordination for $Na_5(SO_3CH_3)_4(X)$ where X = (I) $[BF_4]^-$, (II) $[ClO_4]^-$, (III) $[PF_6]^-$, and (IV) $[I]^-$, (B) deconvolution of the disordered tetrahedral (top) and octahedral (bottom) fragments, and (C) a partial 1D-slice of the edge-sharing $[Na_5(SO_3CH_3)_4]_n^+$ layers that comprise **I–V**.

The primary structural motif in **I–V** are the $[Na_5(SO_3CH_3)_4]_n^+$ layers that are comprised of edge-sharing and distorted NaO_6 octahedra with bridging $[SO_3CH_3]^-$. A 1D-slice of this motif is shown in Fig. 3A. In **I–IV**, the $[Na_5(SO_3CH_3)_4]_n^+$ layers remain largely unchanged. For example, the shortest, longest, and average Na–O bond lengths in **I–V** are all within 2.30(2) Å, 2.84(2) Å, and 2.49(1) Å, respectively. The intralayer $[SO_3CH_3]^-$ anions are similarly unaffected by the substitutions with S–O and S–C bond lengths of 1.453(4) Å and 1.753(3) Å, all consistent with the reported crystal structure for **V**.[24] In **V**, the distorted and polar $[SO_3CH_3]^-$ tetrahedra align in an antipolar arrangements between each layer yielding an overall centrosymmetric crystal structure. The disordered anionic groups fall into two categories. The first are the tetrahedral (**I**) $[BF_4]^-$, (**II**) $[ClO_4]^-$, units, shown in Fig. 3A (top). In **I** and **II**, the nonpolar tetrahedra are only bonded on one axis and are free to rotate as there is no hydrogen bonding nor crystalline waters by SCXRD to prevent rotation. The two disordered fragments superimposed form a pseudo-octahedron (Fig. 3B, top), and fill the interlayer space. In **I**, the average Na–F and B–F bond distances are 2.22(8) Å and 1.38(2) Å, respectively, slightly shorter to that of the crystal structure of $NaBF_4$ (ICSD no. 1607866, 2.359 Å and 1.389 Å, respectively). The average Na–O and Cl–O bond distances in **II** are 2.305 Å and 1.362 Å, respectively, similarly slightly shorter to that of the $NaClO_4$ crystal structure (CCDC no. 8103733, 2.45(8) Å and 1.435(3) Å, respectively).

Similarly, **III** which contains the $[PF_6]^-$ octahedral anion that is disordered over two positions forming a pseudo-spherical group (Fig. 3A and B, bottom). The higher symmetry pseudo-spherical disorder in the $[PF_6]^-$ group gives the lattice an additional body-centering (*I*) symmetry element. The average Na–F and P–F bond lengths are 2.4(3) Å and 1.56(2) Å, which is significantly longer than the Na–F bonds but close to the P–F bond lengths in $NaPF_6$ (ICSD no. 90615, 2.262(4) Å and 1.545(4) Å). Therefore, the $[PF_6]^-$ group is not internally distorted and retains its stableconfirmation. In compound **IV** there is no crystallographic disorder since $[I]^-$ is already spherical, however it does not possess the I symmetry since it is slightly distorted off the center position in the interlayer site (Wyckoff position $2c$ in $I2/m$ or $2e$ in $P2/n$). This could be owing to partial iodine sublimation, however, as has been observed in other iodide containing compounds and mentioned above.[40,49,50] In **IV**, the Na–I distance is noticeably longer than the Na–X length in **I–III** and **V** at 3.1975(1) Å but this is consistent with the stable Na–I bond length in the NaI salt (ICSD no. 53823, 3.237(3) Å).

3.2. Thermal stability

There is generally limited available literature data on the thermal decomposition pathways of methanesulfonate salts owing to their complexity and postulated radical intermediates.[51] Presently, there are some decomposition temperatures and residue PXRDs of simple binary metal methanesulfonates and generally decompose from 350–500 °C.[52,53] Owing to this complexity, only the net decomposition and temperatures will be discussed herein for characterization purposes. In each of the compounds **I–V**, the primary mass component is the $[SO_3CH_3]^-$ group, accounting for 60–65 mass%, with each X-group accounting for 15–22 mass%. **I–IV** behave similarly to **V**, albeit at varying temperatures and decomposition pathways likely owing to the enhanced molecular complexity, discussed below (Fig. 4).

The internal standard, **V** (Fig. S8†) is somewhat hygroscopic and loses ~0.2 equivalents of water at 55–60 °C. It decomposes at 435–450 °C into Na_2CO_3 and loses 52.68% of its mass. This is attributed to the nonstoichiometric decomposition of the methanesulfonate group into primarily sulfur in the form of SO_2, consistent with previous literature.[54] PXRD plots of each residue for **I–IV** are shown in Fig. S9.† Similarly, compound **I** is more hygroscopic and loses ~1.6 molar equivalents of adsorbed water from 50–200 °C. Compound **I** decomposes from 450–490 °C into NaF. Therefore, the corresponding mass loss of 67.48% is likely the entire $[SO_3CH_3]^-$ group as well as the $NaBF_4 \rightarrow NaF(s) + BF_3(g)$ in a concerted step. Compound **II** is significantly more hygroscopic, losing ~3.2 equivalents of water at 80–100 °C. It decomposes at 420–435 °C into a mixture of NaCl, Na_2CO_3, and $Na_6(CO_3)(SO_4)_2$ owing to the complete decomposition of the $[ClO_4]^-$ subunit and partial decomposition (18.78 mass%) of the mesylate group. The rate of decomposition of the mesylate unit observed in **I** and **V** is significantly reduced in **II** over the measured range (24.24 mass% *vs.* > 50 mass%), perhaps inhibited by the NaCl presence or a semi-stable intermediate.

Compound **III** is not measurably hygroscopic by TGA but it has three decomposition steps in the range of 360–520 °C. The residue contains Na_2CO_3, $Na_7(PO_4)_2F$, and NaF, suggesting a complete release of sulphur while retaining most of the phosphorous and some fluorine. The decomposition is likely initiated (−36.31%) by the $[PF_6]^-$ group since $NaPF_6$ has lower thermal stability than $NaSO_3CH_3$ (285 °C *vs.* 435 °C, respectively).[55] The second (−6.59%) and third (−19.07%) steps begin

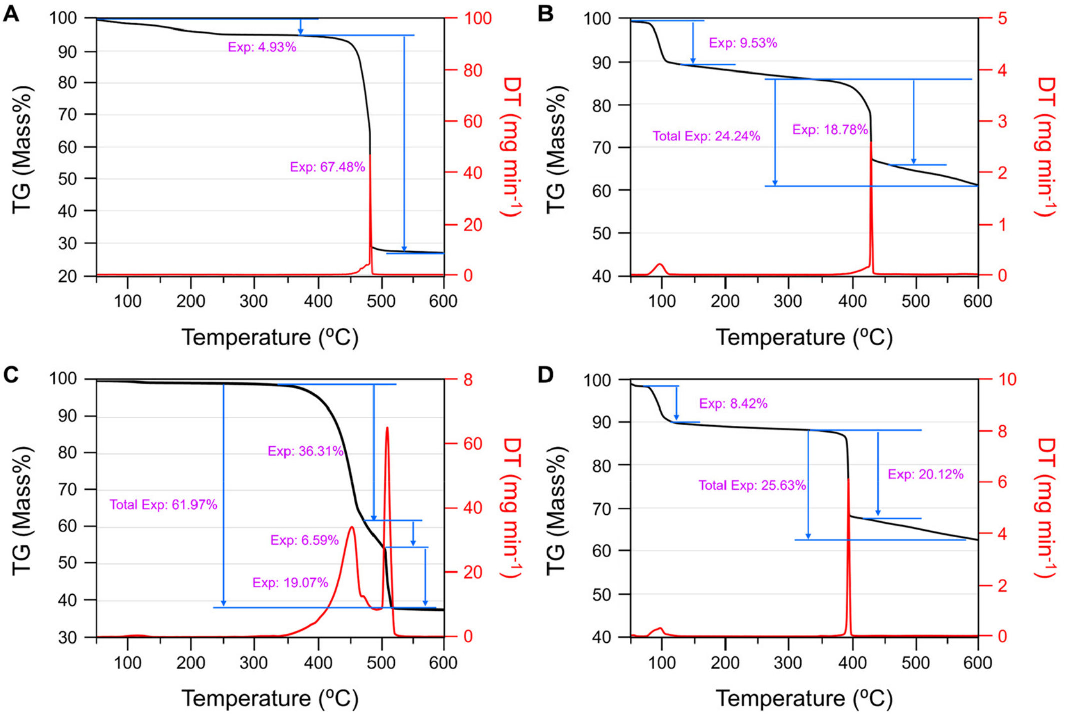

Fig. 4 TGA results for (A–D) **I–IV** from 50–600 °C under N_2 flow. PXRD of each residue and the TGA data for V is shown in the ESI Fig. S8 and S9.†

at 460 °C and 510 °C, respectively. The evolved gases are therefore likely rich in CO_2, SO_2, HF, and H_2O. The pyrolysis products of **IV** were poorly crystallized and more challenging to determine well. Compound **IV** is similarly hygroscopic to **II** and loses 2.9 molar equivalents of water from 50–120 °C. A rapid mass loss of 20.12 mass% occurs at 390 °C which is likely the I (20.4 mass%) as the residue appears to primarily be a mixture of Na_2CO_3–Na_2SO_4 solid solutions, with no crystalline I-containing phases. Additional decomposition of the mixed carbonate-sulfates continues for an additional 5.5 mass% over the measured temperature range. In summary, the relative thermal stability of **I–IV** is similar to **V** and previously reported metal methanesulfonates although the pathways change depending on the X-group. Lastly, the thermal stability of **I–IV** was examined after annealing crystals of each at 300 °C under vacuum. PXRD of the ground crystals are shown in Fig. S11.† **II** and **III** showed no visual change nor significant change by PXRD. Crystals of **I** became opaque and there are some minor changes in peak intensities. **IV** has nearly completely changed structure to another unknown phase.

3.3. Optical properties

The diffuse reflectance spectroscopy results from 200–1200 nm for compounds **I–IV** are shown in Fig. 5 and compound **V** in Fig. S10.† **I–III** and **V** have wide transparencies in the visible region from 400–1100 nm. All four compounds share a weak absorption band at 1170 nm which is common amongst metal methanesulfonates[56] and is also present in **V**. The absorption cutoff edges (λ_{abs}) were estimated from the data as <200 nm for **I** and **III**, 210 nm for **II**, and 230 nm for **IV**. The bandgaps (E_g, Fig. 5 insets) were estimated to be (**I**) 5.4, (**II**) 5.5, (**III**) 5.2, and (**IV**) 4.5, all in eV. Compound **IV** has one lower energy absorption bands from the $[I]^-$ centered at 365 nm, and the cause of the yellow coloration of the crystals. It is likely that the 365 nm band is due to the partial oxidation of the $[I]^-$ in air to I_2 or IO_x^-.[61] For comparison, the λ_{abs} and E_g of **V** were measured to be 210 nm and 5.3 eV, respectively. Despite no change in the $[Na_5(SO_3CH_3)_4]^+$ structural layers, the absorption cutoffs have decreased into the deep-UV (λ < 200 nm) from substitution of $[SO_3CH_3]^-$ for $[BF_4]^-$ and $[PF_6]^-$, no change with $[ClO_4]^-$, and increased to 230 nm with $[I]^-$.

The FT-IR spectra of compounds **I–IV** over the range of 400–4000 cm^{-1} are provided in Fig. 6 and Fig. S10† for **V**. A full list of spectral peak assignments and frequencies has been tabulated in Table S6 in the ESI.† The characteristic peaks from the sodium methanesulfonate structural unit (*i.e.*, C–H, S–O, *etc.*) produce similar FT-IR spectra with minor shifts in frequencies between **I–V** and have been thoroughly investigated elsewhere.[57] In brief, the SO_3 asymmetric and symmetric stretches occur at 1180–1250 cm^{-1} and 1050–1100 cm^{-1}, respectively. The CH_3 asymmetric and symmetric stretches

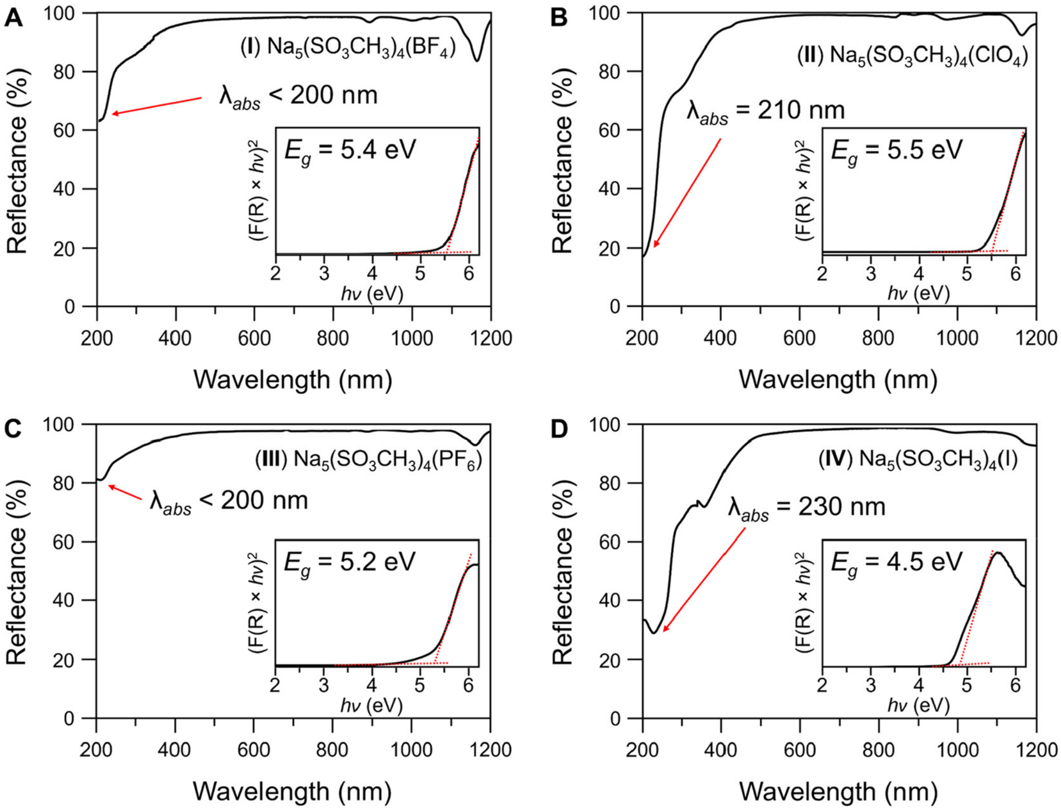

Fig. 5 UV-Vis-NIR diffuse reflectance spectroscopy results for (A–D) **I–IV** from 200–1200 nm. (insets) Tauc plots of the remission function squared. Bandgaps (E_g) were determined by extrapolating to the baseline (red lines).

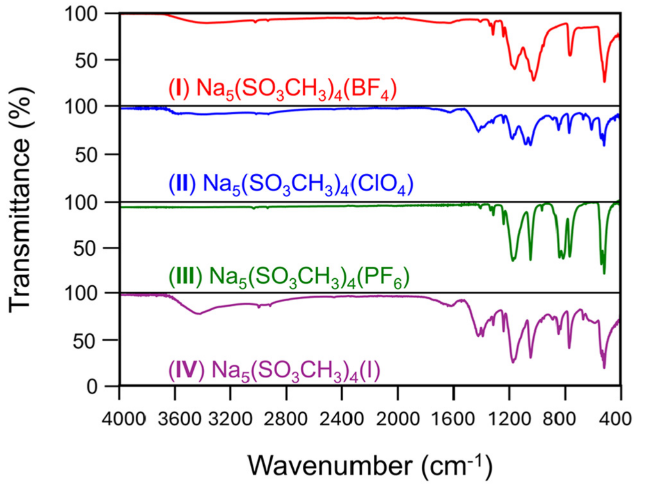

Fig. 6 FT-IR spectroscopy results for I–IV (top to bottom, respectively) from 4000–400 cm^{-1}. FT-IR spectrum for V is in Fig. S10B in the ESI.†

occur at 3000–3050 cm^{-1} and 2940 cm^{-1}, respectively. The bending modes for SO_3 and the SO_3 + CH_3 combination bands are in the 530–800 cm^{-1} region, while the CH_3 bends are centered at 1330–1350 cm^{-1}.

For the new IR peaks observed, **I** has new peaks corresponding to B–F stretches at 1039 and 534 cm^{-1} which overlap with the mesylate vibrations.[58] **II** has a new sharp peak at 635 cm^{-1} from ClO_4 asymmetric bending.[59] **III** similarly has new peaks owing to the PF_6 stretching 858 and 829 cm^{-1}.[60] New peaks emerge from at ~850 and 890 cm^{-1} in **II** and **IV** that are proposed to be water libration, similarly observed in multiple metal sulfonates and hydrates.[57] This is consistent with compounds **II** and **IV** having higher hygroscopicity. Broad bands at 3400–3450 cm^{-1} attributed to water are present in all but compound **III**, which was also observed to be the least hygroscopic and had no water loss in the TGA as described above. No new peaks were observed, nor expected, for Na–I stretching in compound **IV**. These data confirm the crystallographic structure and purity of the crystals obtained and the X-group substitution.

4. Conclusions

The present work investigated using anionic site-substitution as a structure building method to discover new metal methanesulfonates with mixed-anionic groups. Experiments resulted in large crystals of four new compounds, $Na_5(SO_3CH_3)_4(X)$ (X = (**I**) BF_4, (**II**) ClO_4, (**III**) PF_6, and (**IV**) I), each isostructural with the known $NaSO_3CH_3$ salt (X = SO_3CH_3). Compounds **I**, **II**, and **IV** each crystallize in the monoclinic space group *P*2/*n* (no. 13) whereas **III** crystallizes in the monoclinic space group *I*2/*m* (no. 12). The four anionic groups were chosen as they have similar charge density to the $[SO_3CH_3]^-$ anion, and were successfully fully substituted seamlessly into the host $[Na_5(SO_3CH_3)_4]_n^+$ layered substructure. **I–III** have wide optical transparency in the visible-NIR range (400–1200 nm) and **I** and **III** have deep-UV λ_{abs} < 200 nm and **II** has λ_{abs} = 210 nm. **IV** has significant absorption at 350–400 nm due to iodide oxidation in air. **I–IV** have large optical bandgaps of 5.4, 5.5, 5.2, and 4.5, all in eV, respectively. Compounds **I–III** are thermally stable up to 350 °C while **IV** undergoes a phase transition prior to decomposition. The simple synthesis method and resulting >1 cm optical-quality crystals of **I–III** highlights the tuneability of metal methanesulfonate structures and is a promising method for discovering more new compounds with diverse properties.

Author contributions

E.A.G. – conceptualization, data curation, investigation, methodology, writing – original draft, review & editing. P.S.H. – conceptualization, funding acquisition, resources, writing – review & editing.

Data availability

Crystallographic data for **I–IV** has been deposited at the CCDC under accession numbers 2147057–2417060.† The data supporting this article, such as: crystallographic information for **I–IV** including atomic coordinates, BVS calculations, anisotropic parameters, bond lengths, and bond angles; SEM and EDS for **I–V**; PXRD indexing of crystal facets; TGA for **V** and PXRD for residues of **I–V**; UV-Vis DRS for **V** and FT-IR for **I–V**; have been included as part of the ESI.†

Conflicts of interest

There are no conflicts of interest to declare.

Acknowledgements

E. A. G. would like to thank Prof. Xiqu Wang for assistance and discussions with crystal structure refinements. E. A. G. and P. S. H. thank the Welch Foundation (grant E-1457) for their support.

References

1 H. Kageyama, K. Hayashi, K. Maeda, J. P. Attfield, Z. Hiroi, J. M. Rondinelli and K. R. Poeppelmeier, Expanding frontiers in materials chemistry and physics with multiple anions, *Nat. Commun.*, 2018, **9**, 772.
2 K. Maeda, F. Takeiri, G. Kobayashi, S. Matsuishi, H. Ogino, S. Ida, T. Mori, Y. Uchimoto, S. Tanabe, T. Hasegawa, N. Imanaka and H. Kageyama, Recent progress on mixed-anion materials for energy applications, *Bull. Chem. Soc. Jpn.*, 2022, **95**(1), 26–37.

3 C. Chen, Y. Wu and R. Li, The anionic group theory of the non-linear optical effect and its applications in the development of new high-quality NLO crystals in the borate series, *Int. Rev. Phys. Chem.*, 1989, **8**(1), 65–91.

4 J. Cui, C. Li and F. Zhang, Development of mixed-anion photocatalysts with wide visible-light absorption bands for solar water splitting, *ChemSusChem*, 2018, **12**(9), 1872–1888.

5 G. Laurita and R. Seshadri, Chemistry, structure, and function of lone pairs in extended solids, *Acc. Chem. Res.*, 2022, **55**, 1004–1014.

6 S. D. Nguyen, J. Yeon, S. H. Kim and P. S. Halasyamani, BiO(IO_3): A new polar iodate that exhibits an aurivillius-type $(Bi_2O_2)^{2+}$ layer and a large shg response, *J. Am. Chem. Soc.*, 2011, **133**(32), 12422–12425.

7 L. Xiong, J. Chen, J. Lu, C.-Y. Pan and L.-M. Wu, Monofluorophosphates: a new source of deep-ultraviolet nonlinear optical materials, *Chem. Mater.*, 2018, **30**(21), 7823–7830.

8 H. Qiu, F. Li, C. Jin, Z. Yang, J. Li, S. Pan and M. Mutailipu, Fluorination strategy towards symmetry breaking of boron-centered tetrahedron for poly-fluorinated optical crystals, *Angew. Chem.*, 2024, **136**(4), e202316194–e202316202.

9 T. T. Tran, H. Yu, J. M. Rondinelli, K. R. Poeppelmeier and P. H. Halasyamani, Deep Ultraviolet nonlinear optical materials, *Chem. Mater.*, 2016, **28**(15), 5238–5258.

10 K. M. Ok, Towards the rational design of novel noncentrosymmetric materials: factors influencing the framework structures, *Acc. Chem. Res.*, 2016, **49**, 2774–2785.

11 H. Yu, H. Wu, S. Pan, Z. Yang, X. Hou, X. Su, Q. Jing, K. R. Poeppelmeier and J. M. Rondinelli, $Cs_3Zn_6B_9O_{21}$: A chemically benign member of the KBBF family exhibiting the largest second harmonic generation response, *J. Am. Chem. Soc.*, 2014, **136**, 1264–1267.

12 G. Yang, P. Gong, Z. Lin and N. Ye, $AZn_2BO_3X_2$ (A = K, Rb, NH_4; X = Cl, Br): New members of KBBF family exhibiting large SHG response and the enhancement of layer interaction by modified structures, *Chem. Mater.*, 2016, **28**, 9122–9131.

13 Y. Shen, S. Zhao, Y. Yang, L. Cao, Z. Wang, B. Zhao, Z. Sun, Z. Lin and J. Luo, A new KBBF-family nonlinear optical material with strong interlayer bonding, *Cryst. Growth Des.*, 2017, **17**, 4422–4427.

14 C. T. Chen, T. Sasaki, R. K. Li, Y. C. Wu, Z. S. Lin, Y. Mori, Z. G. Hu, J. Wang, G. Aka and M. Yoshimura, *Nonlinear optical borate crystals: principals and applications*, John Wiley & Sons, Weinheim Germany, 2012.

15 B. Xu, P. Gong, F. Liu, X. Zhang, H. Huo and Z. Lin, $(SO_3CF_3)^-$: A non-pi-conjugated motif for nonlinear optical crystals transparent into the deep-ultraviolet region, *Adv. Opt. Mater.*, 2024, **12**(5), 2301725.

16 H. Tian, C. Lin, X. Zhao, F. Xu, C. Wang, N. Ye and M. Luo, $Ba(SO_3CH_3)_2$: A deep-ultraviolet transparent crystal with excellent – optical nonlinearity based on a new polar non-π-conjugated NLO building unit $SO_3CH_3^-$, *CCS Chem.*, 2023, **5**(11), 2497–2505.

17 D. Zagorac, H. Muller, S. Ruehl, J. Zagorac and S. Rehme, Recent developments in the inorganic crystal structure database: theoretical crystal structure data and related features, *J. Appl. Crystallogr.*, 2019, **52**, 918–925.

18 C. Logemann and M. S. Wickleder, The $[Au(CH_3SO_3)_4]^-$ Anion in the crystal structures of $M[Au(CH_3SO_3)_4]$ (M = Li, Na, Rb), *Z. Anorg. Allg. Chem.*, 2012, **638**(10), 1468–1472.

19 M. Liang, Y. Zhang, E. Izvarin, M. J. Waters, J. M. Rondinelli and P. S. Halasyamani, Metal methanesulfonates with mixed anionic groups with large band gaps and enhanced birefringence, *Chem. Mater.*, 2024, **36**(4), 2113–2123.

20 E. A. Gabilondo and P. S. Halasyamani, Synthesis and large crystal growth of a noncentrosymmetric sodium methylsulfanetriol borate lews-adduct: $Na(S(OH)_3CH_3)(BO_3)$, *Inorg. Chem.*, 2024, **63**(37), 17208–17214.

21 S. F. Parker, E. J. Revill-Hivet, D. W. Nye and M. J. Gutmann, Structure and vibrational spectroscopy of lithium and potassium methanesulfonates, *R. Soc. Open Sci.*, 2020, **7**, 200776–200787.

22 R. Uppuluri, A. S. Gupta, A. S. Rosas and T. E. Mallouk, Soft chemistry of ion-exchangeable layered metal oxides, *Chem. Soc. Rev.*, 2018, **47**, 2401–2430.

23 E. A. Gabilondo, S. O'Donnell, R. Newell, R. Broughton, M. Mateus, J. L. Jones and P. A. Maggard, Renaissance of topotactic ion-exchange for functional solids with close packed structures, *Chem. – Eur. J.*, 2022, **28**(33), e202200479–e202200484.

24 C. H. Wei and B. E. Hingerty, Structure of sodium methanesulfonate, *Acta Crystallogr., Sect. B*, 1981, **37**, 1991–1997.

25 *Bruker APEX2*, Bruker AXS Inc., Madison, WI, USA, 2003.

26 G. M. Sheldrick, *SAINT, XPREP (Version 2008/2)*, Bruker AXS Inc., Madison, WI, USA, 2008.

27 R. H. Blessing, An empirical correction for absorption anisotropy, *Acta Crystallogr., Sect. A:Found. Crystallogr.*, 1995, **51**, 33.

28 G. M. Sheldrick, SHELXT-Integrated space-group and crystal-structure determination, *Acta Crystallogr., Sect. A: Found. Adv.*, 2015, **71**, 3–8.

29 G. M. Sheldrick, Crystal structure refinement with SHELXL, *Acta Crystallogr., Sect. C:Struct. Chem.*, 2015, **71**, 3–8.

30 G. M. Sheldrick, A Short History of SHELX, *Acta Crystallogr., Sect. A:Found. Crystallogr.*, 2008, **64**, 112–122.

31 O. V. Dolomanov, L. J. Bourhis, R. J. Gildea, J. A. K. Howard and H. Puschmann, OLEX2: A complete structure solution, refinement and analysis program, *J. Appl. Crystallogr.*, 2009, **42**, 339–341.

32 A. L. Spek, Single-Crystal Structure Validation with the Program PLATON, *J. Appl. Crystallogr.*, 2003, **36**, 7–13.

33 Y. Le Page, Computer derivation of the symmetry elements implied in a structure description, *J. Appl. Crystallogr.*, 1987, **20**, 264–269.

34 Y. Le Page, MISSYM 1.1 – a flexible new release, *J. Appl. Crystallogr.*, 1988, **21**, 983–984.

35 I. D. Brown, Recent developments in the methods and applications of the bond valence model, *Chem. Rev.*, 2009, **109**(12), 6858–6919.

36 IUCr Crystallographic Data on Bond Valence Parameters page. **https://www.iucr.org/resources/data/datasets/bond-valence-parameters**, (accessed 2024-06-06).

37 C. R. Groom, I. J. Bruno, M. P. Lightfoot and S. C. Ward, The Cambridge Structural Database, *Acta Crystallogr., Sect. B:Struct. Sci., Cryst. Eng. Mater.*, 2016, **72**, 171–197.

38 G. Brunton, Refinement of the structure of $NaBF_4$, *Acta Crystallogr., Sect. B*, 1968, **24**, 1703–1704.

39 R. Wartchow and H. J. Berthold, Crystal structure of sodium perchlorate, *Z. Kristallogr.*, 1978, **147**, 307–317.

40 K. F. Tebbe and U. Georgy, Die kristallstrukturen von rubidiumtriiodid und thalliumtriiodid, *Acta Crystallogr., Sect. C:Cryst. Struct. Commun.*, 1986, **42**, 1675–1678.

41 K. Momma and F. Izumi, VESTA 3 for three-dimensional visualization of crystal, volumetric, and morphology data, *J. Appl. Crystallogr.*, 2011, **44**, 1272–1276.

42 P. Kubelka and F. Munk, An article on optics of paint layers, *Z. Tech. Phys.*, 1931, **12**, 593–603.

43 E. L. Simmons, Reflectance spectroscopy: application of the Kubelka-Munk theory to the rates of photoprocesses of powders, *Appl. Opt.*, 1976, **15**, 951–954.

44 J. Tauc, *Amorphous and Liquid Semiconductors*, Springer International Publishing, London, UK, 1974.

45 I. Krossing and I. Raabe, Noncoordinating anions – fact or fiction? A survey of likely candidates, *Angew. Chem., Int. Ed.*, 2004, **43**, 2066–2090.

46 L. H. Ahrens, *Geochim. Cosmochim. Acta*, 1952, **2**(3), 155–169.

47 H. D. B. Jenkins and K. P. Thankur, Reappraisal of thermochemical radii for complex ions, *J. Chem. Educ.*, 1979, **56**(9), 576–577.

48 A. L. Rohl and D. M. P. Mingos, The size and shape of molecular ions and their relevance to the packing of the hexafluorophosphate salts, *Dalton Trans.*, 1992, **24**, 3541–3552.

49 R. C. L. Mooney, The configuration of the triiodide group in ammonium triiodide crystals, *Z. Kristallogr. – Cryst. Mater.*, 1937, **90**(1–6), 143–150.

50 G. H. Cheesman and A. J. T. Finney, Refinement of the structure of ammonium triiodide, NH_4I_3, *Acta Crystallogr., Sect. B*, 1970, **26**, 904–906.

51 J. Cao, W.-L. Wang, L.-J. Gao and F. Fu, Mechanism and thermodynamic properties of CH_3SO_3 decomposition, *Acta Phys.-Chim. Sin.*, 2013, **29**(6), 1161–1167.

52 F. Charbonnier, Thermal behavior of some compounds of methanesulfonic acid with transition metals, *Thermochim. Acta*, 1979, **33**, 31–39.

53 M. Wang, Z. G. Song, H. Hiang and H. Gong, Thermal decomposition of metal methanesulfonates in air, *J. Therm. Anal. Calorim.*, 2009, **98**, 801–806.

54 F. Charbonnier, Study of some alkaline salts of alcanemonosulfonic and alcanedisulfonic acids, *Ann. Chim.*, 1971, **6**(6), 405–411.

55 T. C. Ehlert and M.-M. Hsia, Thermal decomposition of alkali metal hexafluorophosphates, *J. Chem. Eng. Data*, 1972, **17**(1), 18–21.

56 G. Andreev, N. Budantseva and A. Fedoseev, Crystal structure and spectral properties of Np(VI) and U(VI) methanesulfonates, *J. Radioanal. Nucl. Chem.*, 2019, **320**, 485–490.

57 S. F. Parker and L. Zhong, Vibrational spectroscopy of metal methanesulfonates: M = Na, Cs, Cu, Ag, Cd, *R. Soc. Open Sci.*, 2018, **5**, 171574–171573.

58 O. Zavorotynska, M. Corno, A. Damin, G. Spoto, P. Ugliengo and M. Baricco, Vibrational properties of MBH_4 and MBF_4 crystals (M = Li, Na, K): a combined DFT, infrared, and raman study, *J. Phys. Chem. C*, 2011, **115**, 18890–18900.

59 Y. Chen, Y. H. Zhang and L. J. Zhao, ATR-FTIR spectroscopic studies on aqueous $LiClO_4$, $NaClO_4$, and $Mg(ClO_4)_2$ solutions, *Phys. Chem. Chem. Phys.*, 2004, **6**(3), 537–542.

60 A. M. Heyns, The I.R. and raman spectra of sodium hexafluorophosphate monohydrate, $NaPF_6 \cdot H_2O$, *Spectrochim. Acta*, 1977, **33**, 315–322.

61 N. N. Kazantseva, A. Ernepesova, A. Khodjamamedov, O. A. Geldyev and B. S. Krumgalz, Spectrophotometric analysis of iodide oxidation by chlorine in highly mineralized solutions, *Anal. Chim. Acta*, 2002, **456**, 105–119.